Observations of Electromagnetic Fields and Plasma Flow in Hohlraums with Proton Radiography

C. K. Li, F. H. Séguin, J. A. Frenje, and R. D. Petrasso
Plasma Science and Fusion Center, Massachusetts Institute of Technology, Cambridge, Massachusetts 02139, USA

P. A. Amendt, R. P. J. Town, O. L. Landen, and J. R. Rygg
Lawrence Livermore National Laboratory, Livermore, California 94550, USA

R. Betti,* J. P. Knauer, D. D. Meyerhofer,* and J. M. Soures
Laboratory for Laser Energetics, University of Rochester, Rochester, New York 14623, USA

C. A. Back, J. D. Kilkenny, and A. Nikroo
General Atomics, San Diego, California 92186, USA
(Received 28 January 2009; published 18 May 2009)

We report on the first proton radiography of laser-irradiated hohlraums. This experiment, with vacuum gold (Au) hohlraums, resulted in observations of self-generated magnetic fields with peak values $\sim 10^6$ G. Time-gated radiographs of monoenergetic protons with discrete energies (15.0 and 3.3 MeV) reveal dynamic pictures of field structures and plasma flow. Near the end of the 1-ns laser drive, a stagnating Au plasma (~ 10 mg cm^{-3}) forms at the center of the hohlraum. This is a consequence of supersonic, radially directed Au jets (~ 1000 μm ns^{-1}, $\sim$Mach 4) that arise from the interaction of laser-driven plasma bubbles expanding into one another.

DOI: 10.1103/PhysRevLett.102.205001 PACS numbers: 52.38.Fz, 52.30.−q, 52.50.Jm, 52.57.−z

A high-Z enclosure, i.e., hohlraum, creates an environment filled with a nearly blackbody (Planckian) radiation field when irradiated by high-power lasers or energetic ions [1,2]. The cavity generates intense thermal x rays at a radiation temperature (T_r) of hundreds of eV. Hohlraums have been extensively used as radiation sources or platforms for a wide range of basic and applied physics experiments. In studies of laboratory astrophysics and high-energy-density (HED) physics [3,4], for example, hohlraums are used for creating and simulating various extreme HED conditions, including those of stellar and planetary interiors. The hohlraum radiation field is used to compress spherical capsules, through capsule ablation, to high temperature and density in indirect-drive inertial confinement fusion [1,2].

The use of hohlraums requires an understanding of physics details, such as coupling efficiency, plasma conditions, instabilities, radiation uniformity [1,2,5,6], and cavity shape [1,2,7,8]. Electric (E) and magnetic (B) fields generated by several processes may have important effects on hohlraum physics and overall performance [9]. B fields inside a hohlraum can reduce heat flow, since cross field thermal conductivity is modified by a factor of $(1 + \omega_{ce}^2\tau^2)^{-1}$, where ω_{ce} is the electron gyrofrequency and τ is the collision time [10,11]. E fields may modify the plasma conditions and, if sufficiently large, could enhance thick-target bremsstrahlung at x-ray energies well above the Planckian background.

For low-intensity laser drive, such as used in most hohlraum experiments [1–9], the dominant source for B-field generation is expected to be nonparallel electron density (n_e) and temperature (T_e) gradients ($\nabla n_e \times \nabla T_e$) [10,11]. The E field is expected to result from electron pressure gradients (∇P_e) [10,11]. Despite such expectations, prior to this work, no direct experimental measurement and characterization of such hohlraum fields have been made.

The first observations of E and B fields and their evolution in hohlraums, made with time-gated monoenergetic proton radiography [12], are presented in this Letter. Coupled plasma flow dynamics were also observed. Simultaneous imaging with two discrete proton energies breaks any inherent degeneracy between E and B.

In the radiography setup (Fig. 1) the backlighter is a D^3He-filled, thin-glass-shell target driven by 21 OMEGA laser beams [13], producing a $\sim$130-ps-long pulse of 15-MeV D^3He protons and 3.3-MeV DD protons. Imaging detectors utilized CR-39 [14], and the backlighter isotropy allowed two experiments to be performed simultaneously. Each hohlraum had a 30-μm-thick gold wall, 100% laser entrance holes, 2.4-mm diameter, and 2-mm length. Each was driven by 10 laser beams (incidence angle 58.8°) forming a single irradiation ring with total laser energy $\sim$4 kJ in a 1-ns square pulse. The individual beams had full spatial and temporal smoothing [15]. SG4 phase plates resulted in each beam illuminating an elliptical spot on the wall with a ratio of long-to-short axis $\sim$1.2 and laser intensity $\sim 2 \times 10^{14}$ W cm^{-2}. A nickel mesh (60 μm thick, 150-μm hole-to-hole spacing, and 75-μm square holes) [12] divided backlighter protons into discrete beam-

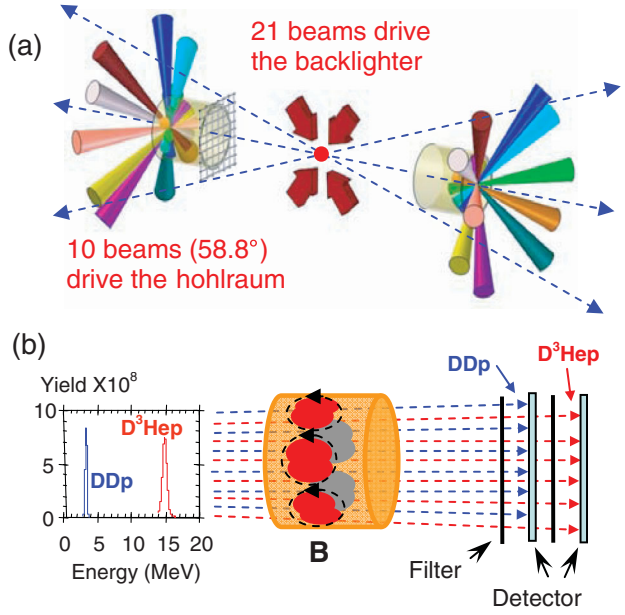

FIG. 1 (color). Experimental setup (a), with proton backlighter, subject hohlraums, and laser beams. The distance between the backlighter and the mesh (detector) was 0.7 (27) cm. Typical energy spectrum and detector are shown in (b). Filters in the detector pack were carefully chosen so that 3.3- and 15-MeV protons were recorded on the front and back detectors, respectively, [14].

lets to allow quantitative measurement of proton trajectory deflection due to fields. The relative timing of backlighter and subject hohlraum drive was adjusted [12] to sample the hohlraum at a desired time.

Figure 2 shows sequences of proton images obtained on three different shots, covering a time period from the beginning of the laser pulse ($t = 0$ ns) to 0.8 ns after it was off ($t \approx 1.8$ ns). At earlier times ($t \leq 0.9$ ns) the beamlet arrays in 15-MeV images [Fig. 2(a)] show minimal displacement by fields or plasma, but beamlets have different sizes at different times, reflecting more subtle field effects. At late times the 15-MeV beamlets show some chaotic spatial structure, indicating that their trajectories have been affected by large field and plasma effects. In the 3.3-MeV images [Fig. 2(b)], beamlet arrays are coherently distorted by $t = 0.52$ ns and disappear altogether (due to stronger deflections) at later times.

Angular deflection of each beamlet is proportional to both $\int \boldsymbol{B} \times d\ell$ and $\int \boldsymbol{E} \times d\ell$ (where $d\ell$ is the differential path length along the proton trajectory), and can be determined from ξ, the linear displacement of a beamlet in an image from the position it would have had in the absence of deflections (we use the apparent size of the displacement scaled to the imaged subject). For certain situations with enough symmetry, the potential degeneracy between E and B can be broken [16,17]. Here this is overcome by near-simultaneous 3.3 and 15 MeV radiographs. Because of the Lorentz force, deflections due to B are inversely proportional to the square root of proton energy ($\xi \propto \varepsilon_p^{-1/2}$) while those due to E are inversely proportional to proton energy ($\xi \propto \varepsilon_p^{-1}$). Measuring beamlet displacements in images from a single shot with these distinct proton energies (ignoring small flight time differences) breaks the degeneracy.

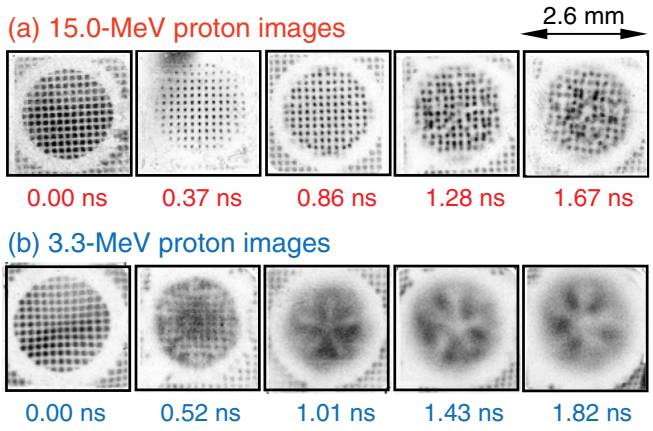

FIG. 2 (color online). Radiographs of a laser-driven Au hohlraum at different times, taken with 15.0-MeV (a) and 3.3-MeV protons (b), illustrating spatial structure and time evolution of proton deflection and beamlet size. Pairs of images in (a) and (b) were taken in the same shot, but represent different sample times due to different proton velocities. In each image, darker means higher fluence; the gray scale mapping is different in each image to account for the different backlighter yields.

The lineouts in Fig. 3 show that the beamlets are approximately uniformly spaced in the hohlraum center re-

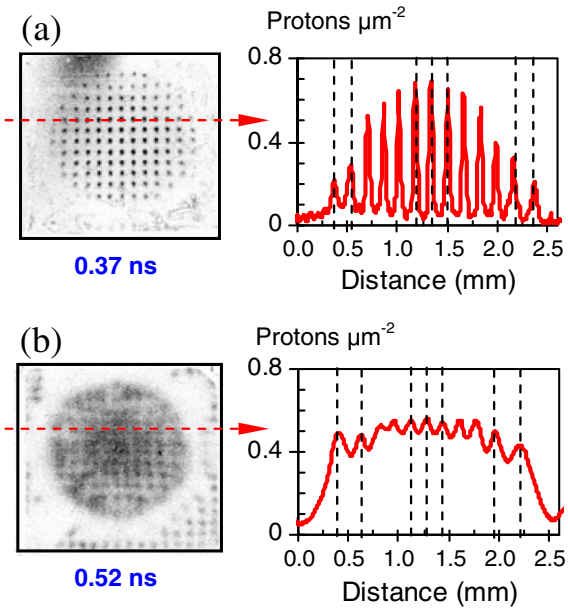

FIG. 3 (color online). Lineouts indicate that the arrays of beamlets are slightly expanded in proximity to the hohlraum wall; displacements ξ are ~ 30 μm and ~ 75 μm for 15-MeV (a) and 3.3-MeV (b) protons, respectively.

gion for both 15-MeV [Fig. 3(a)] and 3.3-MeV protons [Fig. 3(b)], but that they expand, by different amounts in the proximity of the hohlraum wall. The displacements are estimated to be $\approx 30\ \mu$m for 15-MeV protons and $\approx 75\ \mu$m for 3.3-MeV protons. These displacements have a ratio $75/30 \sim 2.5$, which is close to the square root of the energy ratio $(15/3.3)^{1/2} \approx 2.2$ expected from B-field deflection, but far from the energy ratio $(15/3.3) \approx 4.6$ expected from E-field deflections. This comparison suggests that the B field is the dominant source for the observed proton deflections near the hohlraum wall.

Estimating the absolute magnitude of B field involves consideration of the proton trajectories near the hohlraum wall, where they encounter two regions of B field with opposite signs, $\boldsymbol{B}_1$ and $\boldsymbol{B}_2$, as they pass through the two sides of a laser-generated bubble. The deflections in the two regions do not quite cancel because the trajectories of the protons are not exactly parallel to the axis of the hohlraum, so $\delta B \equiv |\boldsymbol{B}_2 - \boldsymbol{B}_1|$ is not zero. We can infer δB from the net beamlet displacement using the formula $\delta B \propto \xi \varepsilon_p^{1/2} L_B^{-1}$ [12], where $L_B \sim L_T \equiv T_e(\nabla T_e)^{-1}$ is the temperature scale length which is about the radius of the plasma bubble ($\sim$200–400 μm). Using either $\xi \sim 30$ (for $\varepsilon_p = 15$ MeV) or $\xi \sim 75\ \mu$m (for $\varepsilon_p = 3.3$ MeV) implies $\delta B \sim 0.1$ MG. To estimate B from δB, we use a result from a 2D LASNEX radiation-hydrodynamic simulation [18], which indicates that $\delta B/B \sim 0.1$; whence it follows that $B \sim 1$ MG.

Electrical charging of the hohlraum, which is electrically connected to the Ni mesh, is indicated by the apparent hole-size reduction seen most clearly in the 15 MeV radiograph at 0.37 ns and the lineout plotted in Fig. 4(a) (symmetry requires that this apparent constriction is an E-field effect). The E field must be associated with gradients in the electrical potential around the mesh holes (on the incoming side only, since the hohlraum acts as a Faraday cage). It can be estimated from a simple formula based on the experimental geometry: $E \approx 4\varepsilon_p q^{-1} L_E^{-2} \Delta$, where $\Delta \approx 0.5A(D - \varpi)L_E a^{-1}(A - a + L_E)^{-1}$ is the apparent displacement at the mesh plane, D is the mesh hole spacing (75 μm), ϖ is the width (FWHM) of a beamlet in the image, a (A) is the distance from backlighter to mesh (detector), q is the proton charge, and L_E is the field scale length. Protons see a transverse field mainly as they enter a mesh hole, and the scale length along their trajectory is about the transverse size of the hole, or 75 μm. The field estimates for different times are plotted in Fig. 4(b), showing that a peak E field $\sim 2 \times 10^9$ V m^{-1} occurs at $\sim$0.37 ns. Interestingly, the field decays away, a likely consequence of discharging, even while the laser drive is on [Fig. 4(b)]. Similar charging and discharging effects have been seen for (arbitrary) targets irradiated by lasers of this intensity. It is this effect that, for thin-glass-shell targets of the experiments described herein and elsewhere [19], caused a slight upshift in the nuclear fusion birth energy from 3.0 (14.7) to 3.3 (15.0) MeV.

A striking feature in Fig. 2 is a five-prong, asterisklike fluence pattern in the 3.3-MeV proton images at $t \geq 1.01$ ns and later. This is a direct consequence of the staggered distribution of laser beams on the hohlraum wall. The 10 beams are grouped in five pairs, with 26.8° between two beams in each pair and 45.2° between adjacent pairs [Fig. 5(a)]. For the experimental conditions ($T_e \sim 1$ keV, $T_i \sim 1$ eV, and $n_e \sim 0.1 n_c$), the plasmas have a high β ($\equiv 8\pi n_e k T_e B^{-2} \sim$ 10–100) and a sound speed [$C_s \sim (ZT_e m_i^{-1})^{1/2} \sim$ 200–300 μm ns^{-1}] that sets a scale for hydrodynamic expansion [20]. With $\sim$200 μm between pairs of bubbles [Fig. 5(a)], it is expected that adjacent bubbles should coalesce in $\sim$0.35 ns and reach the hohlraum axis in $\sim$3–4 ns. In contrast the 3.3 MeV radiograph at 1.01 ns indicates, on the basis of the five-prong asterisk pattern extending to the axis, that Au-plasma jets shoot inward at about $\sim$Mach 4 ($\sim$1000 μm ns^{-1}). The 3.3-MeV radiograph at 1.43 ns

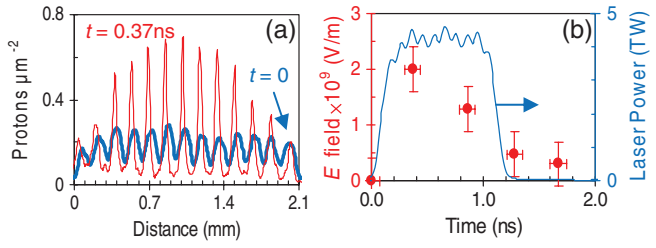

FIG. 4 (color). (a) Lineouts from 15-MeV images [Fig. 2(a)] at two times and (b) E fields estimated from measurements (solid circles).

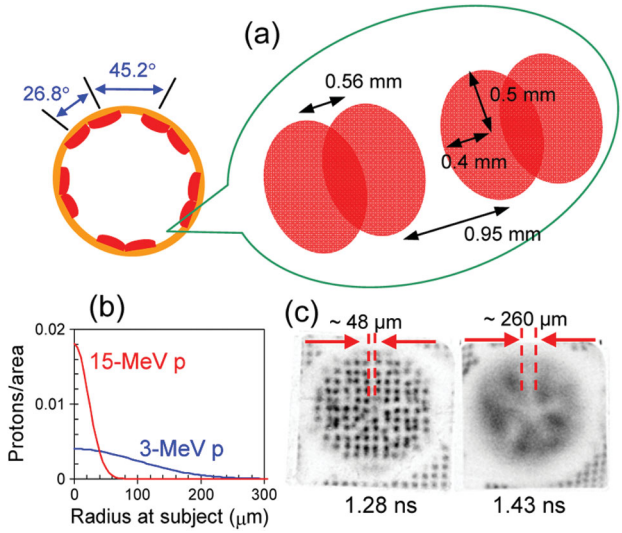

FIG. 5 (color). Laser beam distribution (a), and calculated proton scattering distributions for $a \sim 1$ mg cm^{-2} Au plasma (b), showing that scattering widths for 3- and 15-MeV protons are comparable with the measured widths (c) of the stagnating plasma.

shows a more enhanced asterisk pattern. A faint outline of the same pattern is seen in the corresponding 15-MeV radiograph (at 1.28 ns). From this latter set of radiographs [Fig. 5(c)], the width of the proton-fluence depletion region in a spoke of the asterisk is ~50 (260) μm for the 15 (3.3) MeV protons. If depletion is a result of scattering in the Au plasma, its density can be estimated. Figure 5(b) shows the effects of scattering calculated for 3.3 and 15 MeV protons in a 1-mg cm^{-2} Au plasma. As the scattering width varies inversely with the proton energy [21], the 3.3 MeV scattering profile is broader by about a factor of 5. The observations [Fig. 5(c)] for both the 3.3 and 15 MeV protons are consistent with 1 mg cm^{-2} Au areal density [22,23]. Taking the scale size for the Au plasma (in the direction of the hohlraum axis) to be ~1 mm, the Au density is ~10 mg cm^{-3}.

To explore aspects of these intrinsic 3D phenomena, highly resolved 1D LASNEX radiation-hydrodynamic simulations were run with the Au-plasma bubble expanding into an ultralow density vacuum. These simulations indicate an expansion rate almost comparable to the jets. In addition to this pure hydrodynamic expansion, the hot electrons advancing ahead of the rarefaction expansion could further boost the motion of the Au ions by the ion sound speed. Work is in progress to assess whether such a hybrid motion of the Au bubble is sufficient to generate a nearly 10 mg cm^{-3} stagnation density on the symmetry axis by ~1 ns.

In summary, we report on the first observations of self-generated fields associated with laser-irradiated hohlraums. Discrete but disparate monoenergetic proton energies enable discrimination between E and B fields. Peak B fields were ~10^6 G. Gold plasma (~10 mg cm^{-3}) stagnates on the hohlraum axis by 1 ns due to ~Mach 4 ($v \sim 1000$ μm ns^{-1}) jets that form between adjacent laser-generated plasma bubbles. (Note that this should not occur in an ignition hohlraum, where a gas fill would impede the jets.) These experimental results have important implications for understanding the precise conditions and plasma dynamics inside vacuum hohlraums and provide an impetus for the further development of 3D multifluid codes with self-consistent field generation.

The authors thank Dr. L. J. Suter and Dr. S. H. Glenzer of LLNL for useful discussions. The work was performed at the LLE National Laser User's Facility (NLUF), and was supported in part by U.S. DOE (DE-FG52-07NA28059 and DE-FG52-06N826203), LLNL (B543881 and LDRD-08-ERD-062), LLE (414090-G), the Fusion Science Center at University of Rochester (412761-G), and General Atomics (DE-AC52-06NA27279).

*Also at: Department of Mechanical Engineering, and Physics and Astronomy, University of Rochester, Rochester, NY 14623, USA.

[1] J. D. Lindl, *Inertial Confinement Fusion* (Springer-Verlag, New York, 1999).
[2] S. Atzeni and J. Meyer-Ter-Vehn, *The Physics of Inertial Fusion* (Clarendon, Oxford 2004).
[3] R. P. Drake, *High-Energy-Density Physics* (Springer, New York, 2006).
[4] B. A. Remington *et al.*, Science **284**, 1488 (1999).
[5] L. J. Suter *et al.*, Phys. Rev. Lett. **73**, 2328 (1994).
[6] M. D. Rosen *et al.*, Phys. Rev. E **72**, 056403 (2005).
[7] P. Amendt *et al.*, Phys. Plasmas **14**, 056312 (2007); M. Vandenboomgaerde *et al.*, Phys. Rev. Lett. **99**, 065004 (2007).
[8] P. A. Amendt *et al.*, Phys. Plasmas **15**, 012702 (2008).
[9] S. H. Glenzer *et al.*, Phys. Plasmas **6**, 2117 (1999); Phys. Rev. Lett. **87**, 045002 (2001).
[10] S. I. Braginskii, *Review of Plasma Physics 1* (Consultants Bureau, New York, 1965).
[11] M. G. Haines, Phys. Rev. Lett. **78**, 254 (1997).
[12] C. K. Li *et al.*, Phys. Rev. Lett. **97**, 135003 (2006).
[13] J. M. Soures *et al.*, Phys. Plasmas **3**, 2108 (1996).
[14] F. H. Séguin *et al.*, Rev. Sci. Instrum. **74**, 975 (2003).
[15] D. D. Meyerhofer *et al.*, Phys. Plasmas **8**, 2251 (2001).
[16] J. R. Rygg *et al.*, Science **319**, 1223 (2008).
[17] C. K. Li *et al.*, Phys. Rev. Lett. **100**, 225001 (2008).
[18] G. B. Zimmerman and W. L. Kruer, Comments Plasma Phys. Controlled Fusion **2**, 51 (1975).
[19] C. K. Li *et al.*, Phys. Plasmas **7**, 2578 (2000).
[20] C. K. Li *et al.*, Phys. Rev. Lett. **99**, 015001 (2007).
[21] V. L. Highland, Nucl. Instrum. Methods **129**, 497 (1975).
[22] C. K. Li and R. D. Petrasso, Phys. Rev. Lett. **70**, 3059 (1993).
[23] The possibility that the proton depletion seen in the asterisk spokes could be due to E fields in the Au-plasma jets (which would require ~10^9 V m^{-1}), rather than scattering in the jets, cannot be experimentally excluded by comparing measured deflections of protons at 3.3 and 15 MeV because the energy scaling is the same for both effects. But direct evidence for scattering is strong: the 3.3-MeV protons that passed through the spokes had lower measured energies than those passing between the spokes by ~40 keV, which is consistent with the 1 mg cm^{-2} of Au required to generate the spokes through scattering.